

# Crystal structure of the *Escherichia coli* thioesterase II, a homolog of the human Nef binding enzyme

Jia Li<sup>1</sup>, Urszula Derewenda<sup>1</sup>, Zbigniew Dauter<sup>2</sup>, Stuart Smith<sup>3</sup> and Zygmunt S. Derewenda<sup>1</sup>

<sup>1</sup>Department of Molecular Physiology and Biological Physics, University of Virginia, P.O. Box 800736, Charlottesville, Virginia 22908-0736, USA.

<sup>2</sup>National Cancer Institute, Frederick, and National Brookhaven Laboratory, Building 725A-X5, Upton, New York 11973, USA. <sup>3</sup>Children's Hospital Oakland Research Institute, 747 Fifty-Second Street, Oakland, California 94609, USA.

**Here we report the solution and refinement at 1.9 Å resolution of the crystal structure of the *Escherichia coli* medium chain length acyl-CoA thioesterase II. This enzyme is a close homolog of the human protein that interacts with the product of the HIV-1 *Nef* gene, sharing 45% amino acid sequence identity with it. The structure of the *E. coli* thioesterase II reveals a new tertiary fold, a 'double hot dog', showing an internal repeat with a basic unit that is structurally similar to the recently described β-hydroxydecanoyl thiol ester dehydrase. The catalytic site, inferred from the crystal structure and verified by site directed mutagenesis, involves novel chemistry and includes Asp 204, Gln 278 and Thr 228, which synergistically activate a nucleophilic water molecule.**

Thioesterases are ubiquitous and diverse enzymes that have essential roles in such processes as fatty acid and polyketide

biosynthesis<sup>1,2</sup>, bioluminescence<sup>3</sup>, acyl-CoA turnover<sup>4</sup>, and removal of acyl chains from post-translationally palmitoylated or myristoylated proteins, including ion channels, receptors, signal transduction components and cell adhesion molecules<sup>5,6</sup>. To date, only three thioesterases have been structurally characterized by X-ray crystallography, and the available atomic models underscore the diversity of their molecular architecture. The *Vibrio harveyi* myristoyl acyl carrier protein thioesterase<sup>7</sup> involved in bioluminescence, and the mammalian palmitoyl protein thioesterase<sup>8</sup> belong to the well-known α/β hydrolase superfamily, members of which contain a classic Ser-His-Asp triad in the active site. In contrast, the very recently described 4-hydroxybenzoyl-CoA thioesterase<sup>9</sup> has an unusual 'hot-dog' fold, which was first identified in β-hydroxydecanoyl thiol ester dehydrase<sup>10</sup>. The mechanism by which 4-hydroxybenzoyl-CoA thioesterase hydrolyzes the thioester bond is not fully understood<sup>9</sup>.

The *Escherichia coli* genome harbors two genes that code for thioesterases. Thioesterase I is an enzyme with a predicted α/β hydrolase architecture and mechanism<sup>11</sup>, whereas the homotetrameric medium chain acyl-CoA thioesterase II (TEII) has an amino acid sequence unrelated to any structurally characterized protein<sup>12</sup>, although homologs in other prokaryotes have been reported. TEII has been studied for nearly 30 years<sup>13</sup>, but its catalytic mechanism remains an enigma. Based on chemical modification experiments, His 58 has been implicated as one of the active site residues<sup>12</sup>. We have reported crystallization of this protein<sup>14</sup>, but difficulties encountered during the search for heavy atom derivatives precluded earlier structure determination. Recently, interest in this enzyme has increased after a homolog with 45% amino acid sequence identity was identified in human T cells<sup>15,16</sup>. Surprisingly, the human enzyme was found to bind to, and be activated by, the product of the HIV *Nef* gene. It has been shown that in transgenic mice the *Nef* protein alone can cause many of the typical symptoms associated with AIDS<sup>17</sup>.

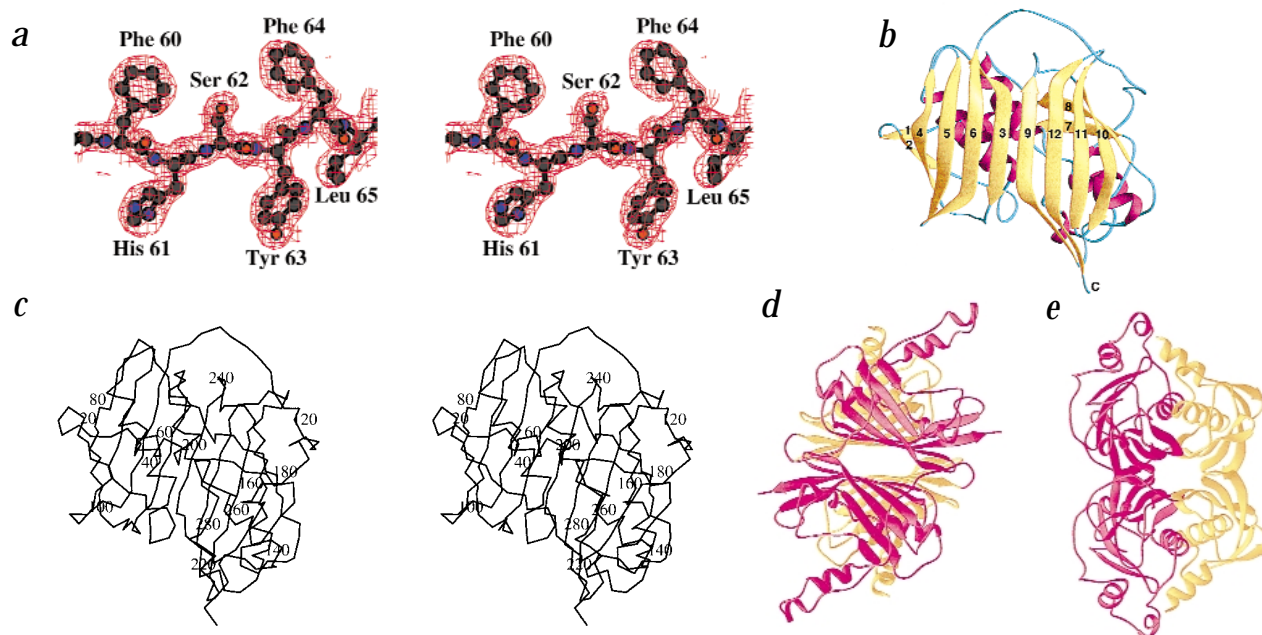


**Fig. 1** The molecular and crystal structure of TEII from *E. coli*. **a**, Representative experimentally phased electron density (MAD, improved in DM) map at 2.5 Å resolution. **b**, Ribbon diagram showing an overview of the tertiary architecture of TEII. The α-helices are magenta, and the central β-sheet is yellow. The residues in each secondary structure element are: α<sub>1</sub>, 4–12; β<sub>1</sub>, 15–18; β<sub>2</sub>, 21–24; α<sub>2</sub>, 36–49; β<sub>3</sub>, 56–64; β<sub>4</sub>, 74–83; β<sub>5</sub>, 87–96; β<sub>6</sub>, 99–109; α<sub>3</sub>, 133–141; β<sub>7</sub>, 158–161; β<sub>8</sub>, 177–180; α<sub>4</sub>, 192–205; β<sub>9</sub>, 224–232; β<sub>10</sub>, 245–254; β<sub>11</sub>, 258–267; β<sub>12</sub>, 272–282. The numbering of β-strands follows their consecutive occurrence along the polypeptide chain. **c**, Stereo view of the Cα trace of the TEII monomer, with every 20<sup>th</sup> residue numbered. **d**, The TEII dimer, with the two repeats in each monomer colored yellow and magenta. **e**, A view of the dimer rotated 90° around the vertical axis relative to (d).

## letters

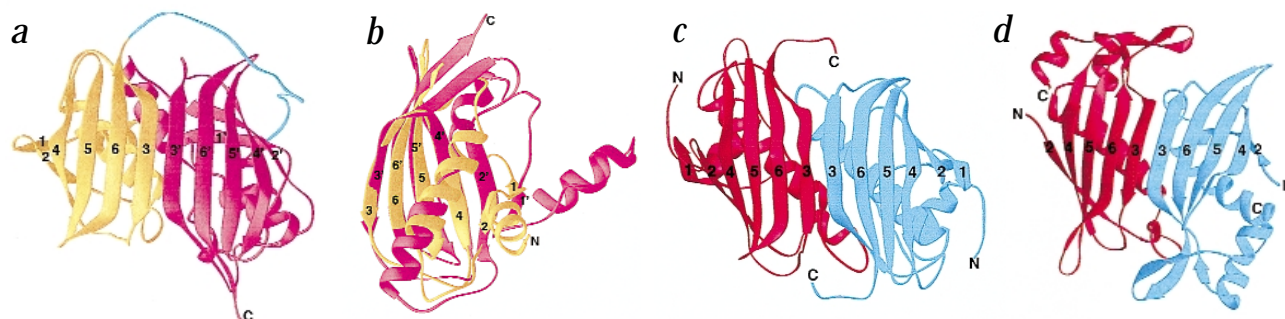


**Fig. 2** The internal structural repeat in TEII and structural similarities with 4-hydroxybenzoyl-CoA thioesterase and  $\beta$ -hydroxydecanoyl thiol ester dehydrase. **a**, TEII, viewed as in Fig. 1*b*, with the two repeats colored yellow and magenta, and the strands numbered consecutively in each repeat so that strands numbered 1'–6' in the second repeat correspond to 1–6 in the first. **b**, Least-squares superposition of the two TEII repeats; this view shows the molecule after a 180° rotation around a vertical axis relative to **a**, to better visualize the fit. The r.m.s. difference for the four central  $\beta$ -strands (3–6) and the central helix is 3.37 Å for C $\alpha$  atoms. **c**, Ribbon diagram of  $\beta$ -Hydroxydecanoyl thiol ester dehydrase (Protein Data Bank (PDB) accession code 1MKB) viewed along the homodimer dyad. The two monomers, corresponding to the repeats in TEII, are colored red and cyan. **d**, Ribbon diagram of the monomer of 4-hydroxybenzoyl-CoA thioesterase (PDB accession code 1BVQ) in an analogous view to (**c**), with two monomers colored accordingly.

Protein–protein interactions involving Nef that occur during the infection of the cell by the HIV are, therefore, of considerable interest. Given the close similarity of the *E. coli* and human thioesterases, the former protein can serve as a plausible model for the human enzyme.

In this paper, we describe the 1.9 Å resolution structure of the *E. coli* TEII. We show that it represents a novel fold, a 'double hot dog', which contains an internal repeat with topology closely resembling  $\beta$ -hydroxydecanoyl thiol ester dehydrase<sup>10</sup> and 4-hydroxybenzoyl-CoA thioesterase<sup>9</sup>. Interestingly, the location of the active site, inferred from the X-ray structure and verified by site directed mutagenesis, coincides with that proposed for  $\beta$ -hydroxydecanoyl thiol ester dehydrase<sup>10</sup>, although the chemistry of catalysis appears to be very different. A triad of Asp 204, Thr 228 and Gln 278 serves to orient a water molecule for a nucleophilic attack on the carbonyl thioester carbon of the incoming substrate.

#### Solution and quality of the structure

The structure of TEII was solved at 2.5 Å resolution by the multi-wavelength anomalous diffraction (MAD) method using data collected at four wavelengths from a single selenomethionine (SeMet) labeled crystal, as described in Methods. After density modification the electron density map was clearly interpretable (Fig. 1*a*), but was improved further by noncrystallographic averaging. The atomic model, which consisted of a noncrystallographic dimer, was then refined against 1.9 Å data collected from a single crystal of the wild type protein to an R-factor and free R<sub>free</sub> (1.5% of data, 1,125 reflections) of 21.8% and 24.8%, respectively (Table 1). The model contains residues 2–286 in each of the two molecules. The loops containing residues 28–33 and 140–155 are largely disordered, and only main chain atoms were modeled into the density. The refined model includes 535 water molecules. Two molecules of LDAO (N, N-dimethyl-dodecylamineoxide) (the detergent used in the crystallization) were modeled into residual positive difference electron density and included in the course of refinement, although this had limited impact on the density. Final refinement was carried out with the LDAO residues omitted to reduce the bias.

The stereochemistry of the final model was analyzed using PROCHECK<sup>18</sup>. Most of the amino acids (91.3%) were found in the most favored regions, while the remaining 8.7% were all in the allowed regions of the Ramachandran plot. Other details are given in Table 1.

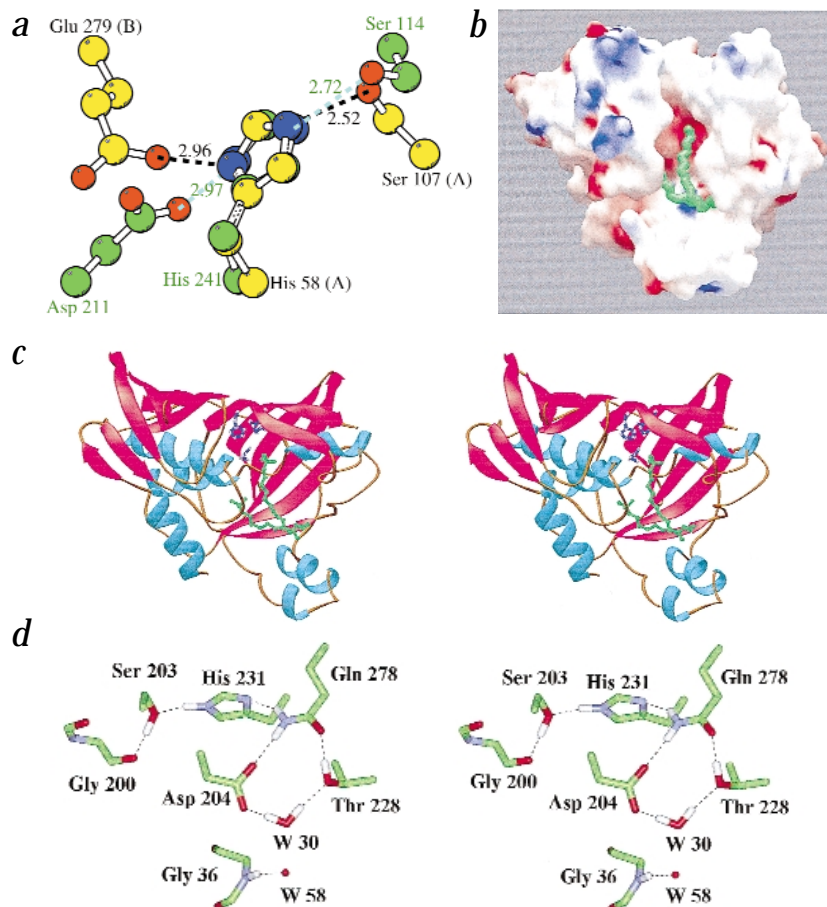
#### TEII exhibits a novel tertiary fold

The TEII monomer has an elliptical shape and dimensions of ~52 Å × 66 Å × 82 Å (Fig. 1*b,c*). It contains a 12-stranded, antiparallel  $\beta$ -sheet with a novel  $\beta$ -sheet topology defined as +1, +4, -3, +1, +1, +7, -1, -4, +3, -1, -1. This topology contains an internal two-fold pseudosymmetry axis perpendicular to the center of the sheet (Fig. 2*a*) such that strands 1–6 can be superimposed on strands 7–12 after a 180° rotation. These two structural repeats are connected by a long loop (residues 110–132) that joins the carboxyl end of strand 6 with strand 7. This exposed loop is susceptible to limited proteolysis (data not shown), further indicating that TEII has a pseudo two-domain structure. Although the structural repeat is strongly suggestive of gene duplication, no sequence similarity is observed between the two halves of the molecule.

A DALI search<sup>19</sup> identified two enzymes with structural similarities to TEII:  $\beta$ -hydroxydecanoyl thiol ester dehydrase<sup>10</sup> and 4-hydroxybenzoyl-CoA thioesterase<sup>9</sup>, both of which are from bacterial sources. No homology could be detected between any of these enzymes at the amino acid sequence level. Moreover, both proteins are smaller than TEII, and structurally similar to only one of the two repeats that constitute the TEII fold (Fig. 2*c,d*). This tertiary fold was first described for  $\beta$ -hydroxydecanoyl thiol ester dehydrase and was named the 'hot dog' fold, as it was noted that the six-stranded  $\beta$ -sheet wraps around a hydrophobic core  $\alpha$ -helix in a manner reminiscent of a bun wrapping around a sausage<sup>10</sup>. In the dehydrase and the 4-hydroxybenzoyl-CoA thioesterase, two monomers associate to form extended  $\beta$ -sheets (12-stranded and 10-stranded, respectively) that are structurally equivalent to that observed in the TEII monomer. We have therefore called the fold in TEII a 'double hot dog'.

The TEII dimer observed in our crystal structure does not have a counterpart in either  $\beta$ -hydroxydecanoyl thiol ester dehydrase or 4-hydroxybenzoyl-CoA thioesterase. The noncrystallographic two-fold axis that relates the two TEII monomers is nearly parallel to the crystallographic *c* axis. Dimerization brings together the exposed surfaces of the  $\beta$ -sheets from the two monomers to form an extensive interface (Fig. 1*d,e*). Specifically, the central fragments of each of the sheets — that is, strands 3, 5, 6 from one and 9, 11, 12 from the other — form this interface. The solvent accessible surface area buried in the dimer interface amounts to 2,146 Å<sup>2</sup> per monomer, a value that suggests that the dimer has a low dissociation constant and is functionally significant.

**Fig. 3** The active site and catalytic mechanism of TEII. **a**, The hydrogen bond network involving His 58, formerly implicated in catalysis, and its comparison with that of the catalytic triad in the C14:ACP thioesterase (an  $\alpha/\beta$  hydrolase) from *V. harveyi* (PDB accession code 1THT; green carbon atoms). **b**, A GRASP surface rendering showing a negatively charged gorge with two bound LDAO molecules. **c**, Ribbon stereo diagram showing the location of the active site residues (colored blue) in relation to the putative substrate binding pocket. **d**, Stereo view of the hydrogen bond network in the active site. W30 is the putative nucleophilic water and has two protons (shown in white) located to optimize the hydrogen bond geometry. Protein protons that can be placed according to stereochemical constraints are all shown. W58 is the water molecule that occupies the putative oxyanion hole.



### His 58 is part of a trypsin-like triad

Although nearly 30 years ago Bonner and Bloch<sup>13</sup> proposed that a carboxylic acid is located in the active site in TEII, biochemical studies have failed to identify the active residues. The only amino acid to be implicated in catalysis was His 58, which was labeled by the inhibitory <sup>14</sup>C-iodoacetamide<sup>12</sup>. The present crystal structure shows that His 58 is located at the dimer interface and that it is hydrogen bonded through N $\epsilon$ 2 to the hydroxyl group of Ser 107, and through N $\delta$ 1 to the carboxyl group of Glu 279 from the adjacent monomer. The relative orientations of the three side chains conform to the paradigm of the trypsin-like catalytic triad<sup>20</sup> (Fig. 3a). Typical catalytic triads consisting of a nucleophilic serine, a histidine and a carboxylic acid (Asp or Glu) have been identified in four diverse families of proteins that have significantly different tertiary folds; in the subtilisin and trypsin families of proteinases,  $\alpha/\beta$ -hydrolases and, most recently, in an intracellular PAF-specific phospholipase A2 (ref. 21). Essentially, all triads conforming to this paradigm perform a catalytic function. We therefore considered the possibility that TEII contains an unusual catalytic triad formed by residues from both monomers across the dimer interface. Indeed, two mutant proteins, S107C and E279Q, showed decreased activity ( $k_{\text{cat}}$  46 s<sup>-1</sup> and 20 s<sup>-1</sup>, respectively, in contrast to 84 s<sup>-1</sup> for the wild type protein, with only a slightly changed  $K_{\text{m}}$ ). Although these results were suggestive, they were not conclusive. The TEII triad has the handedness of a typical serine proteinase, rather than that found in all triad containing lipases and esterases<sup>22</sup>; there was no obvious substrate binding site and no oxyanion hole to stabilize the tetrahedral intermediate formed during catalysis. Moreover, the sequence of yeast TEII lacks both the seryl and histidyl residues of the triad (they are replaced by Leu and Thr, respectively), yet it exhibits catalytic activity similar to its human homolog<sup>23</sup>.

### Novel chemistry at the active site

In an effort to identify the substrate binding site we analyzed the environs of the two LDAO molecules bound in the cavity between two flexible loops (residues 27–33 and 133–155) on one side and the main  $\beta$ -sheet on the other side. The side chain of Asp 204 is at the bottom of the gorge, close to the head group of one of the LDAO molecules (Fig. 3b,c). This residue is hydrogen bonded to the side chain amide of Gln 278, which in turn accepts a proton in a hydrogen bond with the hydroxyl of Thr 228

(Fig. 3d). This hydrogen bonding network creates a water binding site between Asp 204 and Thr 228 in which a solvent molecule (W30) is tightly bound via two hydrogen bonds, with water acting as donor in both. This water molecule is rendered nucleophilic by the proximity of the partly buried Asp 204, and is likely to serve as the attacking hydrolytic water. It is noteworthy that O $\delta$ 2 of Asp 204 (which is 2.6 Å away from the W30 oxygen) is not involved in any other hydrogen bond, which may have otherwise neutralized its negative charge, but instead is shielded by the proximity of the side chain of Phe 35. To further stabilize the Ser-Gln-Asp network, His 231 accepts a hydrogen bond from the side chain amide of Gln 278 via deprotonated N $\delta$ 1, and donates a proton to a hydrogen bond with the hydroxyl group of Ser 203. The latter forms a hydrogen bond with the carbonyl group of Gly 200, donating its own proton. This hydrogen bonding network is unique to the second structural repeat, and has no counterpart in the first.

We probed the functionality of Asp 204 by designing, expressing and assaying two mutants, D204N and D204A. In both cases, the  $k_{\text{cat}}$  was reduced by ~1,000-fold, from 83 s<sup>-1</sup> to 0.085 and 0.076 s<sup>-1</sup>, respectively. The  $K_{\text{m}}$  value did not change significantly (18 and 13  $\mu$ M, respectively, compared to 13  $\mu$ M for the wild type). These data strongly support the notion that Asp 204 has a catalytic function. We also compared all the known amino acid sequences of TEII homologs. All the residues implicated in the new active site are conserved, with the exception of Thr 228. This position is a serine in two members of the family, which still preserves the critical function of the side chain hydroxyl (Fig. 4).

Esterases typically stabilize the tetrahedral intermediates formed during catalysis in a so-called oxyanion hole. The main

## letters

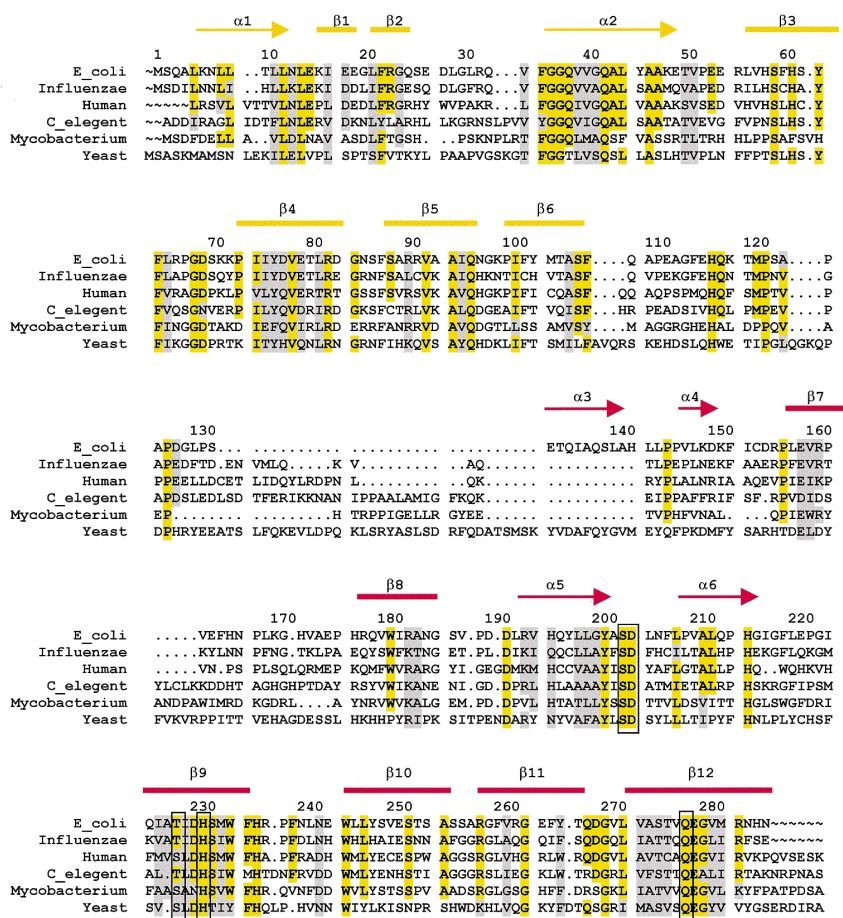


**Fig. 4** Structure based sequence alignment of the TEII family members. Secondary structure elements are shown above the sequences; gold refers to the first repeat, red to the second. Yellow indicates conserved amino acids, gray denotes similarities. Residues involved in the active site are boxed. Blue indicates residues involved in the active site. Note the large insertion in the yeast sequence between the two repeats.

chain amide of Gly 36, which is the second residue in the fully conserved Phe 35-Gly 36-Gly 37 tripeptide, is adjacent to the site occupied by Asp 204 and W30. The location of this amide suggests that it is involved in the catalytic process, and the water molecule bound to it (W58, Fig. 3d) probably occupies the site where the oxyanion binds. Glycine-rich loops often participate in the formation of the oxyanion holes in esterases because the lack of side chains allows for structural flexibility around the substrate binding site. It should be noted that the oxyanion hole in TEII is formed by the first structural repeat, and so the active site is situated near the interface between the two 'hot dog' motifs.

Finally, Asp 204 is likely to serve yet another purpose. Most active sites in esterases and lipases are negatively charged. It is thought that this facilitates the expulsion of the negatively charged reaction product (a free acyl group). We note that TEII also shows negative electrostatic potential in the active site (Fig. 3b), which is conferred almost exclusively by the side chain of Asp 204.

### Conclusion

*E. coli* TEII is a representative of a novel and ubiquitous family of thioesterases, members of which have been found in bacte-

ria, yeast, and humans. The amino acid sequence of this enzyme has been rather stringently conserved throughout evolution, such that the *E. coli* and human proteins are 45% identical, suggesting that it has an important physiological function. The human enzyme has been discovered in T cells, where it is one of the binding targets of the HIV-1 Nef protein, suggesting that it has a possible role in AIDS pathogenesis. We have solved the crystal structure of the *E. coli* TEII, which has a novel fold consisting of two repeats of an  $\alpha/\beta$  motif with a six-stranded antiparallel  $\beta$ -sheet topology. The motif is highly reminiscent of the tertiary structure of the 4-hydroxybenzoyl-CoA thioesterase, although no evidence of homology can be detected at the amino acid level, and the two enzymes apparently operate by different catalytic mechanisms. The active site of TEII shows novel chemistry for a thioesterase; it contains a hydrogen bonding network of several residues, notably a triad of Asp 204, Gln 278 and Thr 228, which orient a water molecule for nucleophilic attack on the substrate. The 1.9 Å resolution structure of the *E. coli* enzyme sets the stage for further analysis of the structure-function relationships in this family of thioesterases, including the determination of the mechanism by which Nef binds to and activates the human enzyme.

### Methods

**Protein expression, crystallization and data collection.** Purification and crystallization of wild type TEII has been reported<sup>14</sup>. For this study, the *tesB* gene was subcloned into a modified pET expression vector<sup>24</sup>. The sequence verified clone was transformed into bacteria expression strain BL21(DE3). Normally, 10 ml of overnight seed culture was used to inoculate 1 l of LB containing 150  $\mu\text{g ml}^{-1}$  ampicillin and the culture was grown to a density of about 0.6–0.8 OD at 600 nm. IPTG (isopropyl  $\beta$ -D-thiogalactopyranoside) was then added to a final concentration of 1 mM and the incubation continued for another 8–12 h. The protein was purified through a Ni-NTA column (Invitrogen). The His-tag was cleaved off with rTEV protease. Crystallization followed the established procedure<sup>14</sup>. Briefly, protein at 6 mg  $\text{ml}^{-1}$  concentration in 20 mM Tris-HCl, pH 7.0, 2 mM dithiothreitol (DTT) was mixed with an equal volume with reservoir solution containing 2 M NaCl, 100 mM NaOAc, pH 6.5 and 5 mM N,N-dimethyl-dodecylamineoxide (LDAO). The sitting drop method was used in a CrystalClear™ stripe to produce large size crystals. Native data were collected from a single crystal to 1.9 Å using a MAR image plate system at the X11 beamline, EMBL outstation, Hamburg. The unit cell ( $a = 95.9 \text{ \AA}$ ,  $b = 119.8 \text{ \AA}$ ,  $c = 165.5 \text{ \AA}$ , C222<sub>1</sub>) was similar to that published<sup>14</sup>. Because of extreme nonisomorphism of the wild type native crystals, attempts to solve the structure using conventional heavy atom derivatives have failed. In order to obtain SeMet crystals suitable for MAD phasing, the TEII protein was overexpressed in the methionine auxotroph B834(DE3) strain. The SeMet labeled protein was purified in the same fashion as the wild type, and crystallized as described for the native protein at slightly higher precipitant concentration. The size of the crystals was significantly enhanced using the sitting drop method and a thin

Table 1 X-ray crystallographic data, phasing and refinement data

	Native	Se-Met( $\lambda$ 1)	Se-Met( $\lambda$ 2)	Se-Met( $\lambda$ 3)	Se-Met( $\lambda$ 4)
$\lambda$ (Å)	0.9096	0.9793	0.9787	0.9747	0.9801
Resolution (Å)	1.90	2.5	2.5	2.5	2.5
Total observations	353,158	153,509	153,931	160,930	206,451
Unique reflections	74,901	33,346	33,397	33,432	33,545
Completeness (%) <sup>1</sup>	99.7(99.4)	99.8(99.9)	99.6(99.8)	99.7(99.8)	99.8(99.7)
R <sub>sym</sub> (%) <sup>2</sup>	5.9(42.5)	4.3(11.6)	4.8(11.5)	4.7(12.5)	4.3(15.5)
Phasing power (acentric / centric) <sup>3</sup>			1.28 / 0.94	1.11 / 0.83	0.89 / 0.59
R <sub>cullis</sub> (acentric / centric) <sup>4</sup>			0.90 / 0.87	0.82 / 0.76	0.91 / 0.92
R <sub>cullis_ano</sub>		0.80	0.72	0.74	0.97
<b>Refinement data</b>		<b>R.m.s. deviations</b>			
Overall figure of merit (20.0 – 2.5 Å) / after DM	0.553 / 0.765	Bond lengths (Å) / Bond angles (°)		0.005 / 1.33	
Resolution used in final refinement (Å)	20.0 – 1.9	B-factors (Å <sup>2</sup> )			
R <sub>cryst</sub> / R <sub>free</sub> (%) <sup>5</sup>	21.8 / 24.8	Main chain / Side chain		1.50 / 2.24	

<sup>1</sup>The numbers in parentheses describe the relevant values for the last resolution shell.

<sup>2</sup>R<sub>sym</sub> =  $\sum |I_i - \langle I \rangle| / \sum I_i$ , where  $I_i$  is the intensity of the  $i$ th observation and  $\langle I \rangle$  is the mean intensity of the reflection;

<sup>3</sup>Phasing power =  $\langle \Delta \text{ano} \rangle / \langle \epsilon \rangle$ ; where  $\langle \Delta \text{ano} \rangle$  is the mean anomalous difference and  $\langle \epsilon \rangle$  is the mean lack of closure.

<sup>4</sup>R<sub>cullis</sub> =  $\sum |\epsilon| / \sum |F_{PH} - F_P|$ , where  $\epsilon$  is lack of closure,  $F_{PH}$  and  $F_P$  are observed derivative and native protein structure factors.

<sup>5</sup>R<sub>cryst</sub> =  $\sum |F_o - F_c| / \sum |F_o|$ ; R<sub>free</sub> =  $\sum |F_o - F_c| / \sum |F_c|$ , where  $F_c$  is the calculated structure factor.

layer of silicon/paraffin oil mixture spread over the drop to reduce the rate of equilibration. Data to 2.5 Å from a single SeMet TEII crystal were collected at four wavelengths at beamline X9B at the National Synchrotron Light Source (Brookhaven National Laboratory). All data were processed with the HKL suite<sup>25</sup>. Details are shown in Table 1.

**Structure determination and model refinement.** Eight Se sites were identified by direct methods using SHELXS<sup>26</sup> (unless otherwise stated the CCP4 suite<sup>27</sup> of programs was used). This immediately suggested that two monomers, rather than a complete tetramer, occupy the asymmetric unit, because there are five possible Met residues in the TEII sequence. The Se coordinates were refined and phases were calculated in MLPHARE, treating the MAD scheme as a special case of MIR (subsequent calculations have shown that the use of single wavelength data, either at the peak or remote high energy, was sufficient to obtain an interpretable map; J.L., unpublished results). Following density modification in DM (CCP4), the electron density map was clearly interpretable. Noncrystallographic two-fold symmetry averaging was carried out in RAVE<sup>28</sup> and a model was built interactively in O<sup>29</sup>. The initial model gave an R-factor of 47% in the resolution range 20–2.5 Å. It was refined to R-factor and R<sub>free</sub> values of 0.26 and 0.30, respectively, without any solvent. This partly refined model was then used as search model in molecular replacement using the 1.9 Å data set. The molecular replacement solution obtained with AmoRe<sup>30</sup> was then refined using CNS<sup>31</sup>. Water molecules were added in CNS and then manually edited based on the difference electron density maps.

**Kinetics assay.** Incubation systems, at 25 °C, contained 50 mM potassium phosphate buffer pH 8, 0.125 mM 5,5'-dithiobis-(2-nitrobenzoate), 20  $\mu$ g ml<sup>-1</sup> bovine serum albumin and enzyme. Reactions were started by the addition of decanoyl-CoA and monitored spectrophotometrically by recording the increase in absorbance at 412 nm. Kinetic parameters were calculated using EnzymeKinetics (Trinity Software).

**Figures.** The figures were prepared using BOBSCRIPT<sup>32</sup>, RIBBONS<sup>33</sup>, GRASP<sup>34</sup> and WebLab ViewerPro (MSI Inc.).

**Coordinates.** The atomic coordinates have been deposited in the Protein Data Bank (accession code 1C8U). They can also be obtained directly from Z.S. Derewenda.

#### Acknowledgments

We thank the EMBL outstation, Hamburg, for providing access to the synchrotron beamlines, and for outstanding assistance. A. Murzin (LMB, Cambridge, UK) was the first to note and point out to us the internal repeat in the structure of TEII. S. Garrard is gratefully acknowledged for conducting limited proteolysis on TEII. This study was funded by the National Institute of General Medical Sciences.

Correspondence should be addressed to Z.S.D. email: [zsd4n@virginia.edu](mailto:zsd4n@virginia.edu)

Received 11 April, 2000; accepted 26 May, 2000.

- Katz, L. & Donadio, S. *Annu. Rev. Microbiol.* **47**, 875–912 (1993).
- Smith, S. *FASEB J.* **8**, 1248–1259 (1994).
- Meighen, E.A. *FASEB J.* **7**, 1016–1022 (1993).
- Waku, K. *Biochim. Biophys. Acta* **1124**, 101–111 (1992).
- Duncan, J.A. & Gilman, A.G. *J. Biol. Chem.* **273**, 15830–15837 (1998).
- Bizzozero, O.A. *Neuropediatrics* **28**, 23–26 (1997).
- Lawson, D.M. *et al. Biochemistry* **33**, 9382–9388 (1994).
- Bellizzi, J.J. *et al. Proc. Natl. Acad. Sci. USA* **97**, 4573–4578 (2000).
- Benning, M.M. *et al. J. Biol. Chem.* **273**, 33572–33579 (1998).
- Leesong, M., Henderson, B.S., Gillig, J.R., Schwab, J.M. & Smith, J.L. *Structure* **4**, 253–264 (1996).
- Cho, H. & Cronan, J.E., Jr. *J. Biol. Chem.* **268**, 9238–9245 (1993).
- Naggert, J. *et al. J. Biol. Chem.* **266**, 11044–11050 (1991).
- Bonner, W.M. & Bloch, K. *J. Biol. Chem.* **247**, 3123–3133 (1972).
- Swenson, L., Green, R., Smith, S. & Derewenda, Z.S. *J. Mol. Biol.* **236**, 660–662 (1994).
- Liu, L.X. *et al. J. Biol. Chem.* **272**, 13779–13785 (1997).
- Watanabe, H. *et al. Biochem. Biophys. Res. Commun.* **238**, 234–239 (1997).
- Hanna, Z. *et al. Cell* **95**, 163–175 (1998).
- Laskowski, R.A., McArthur, M.W., Moss, D.S. & Thornton, J.M. *J. Appl. Crystallogr.* **26**, 282–291 (1993).
- Holm, L. & Sander, C. *J. Mol. Biol.* **233**, 123–138 (1993).
- Wallace, A.C., Laskowski, R.A. & Thornton, J.M. *Protein Sci.* **5**, 1001–1013 (1996).
- Dodson, G. & Wlodawer, A. *Trends Biochem. Sci.* **23**, 347–352 (1998).
- Derewenda, Z.S. & Wei, Y. *J. Am. Chem. Soc.* **117**, 2104–2105 (1995).
- Jones, J.M., Nau, K., Geraghty, M.T., Erdmann, R. & Gould, S.J. *J. Biol. Chem.* **274**, 9216–9223 (1999).
- Sheffield, P., Garrard, S. & Derewenda, Z. *Protein Expr. Purif.* **15**, 34–39 (1999).
- Otwinowski, Z. & Minor, W. *Methods Enzymol.* **A 276**, 307–326 (1997).
- Sheldrick, G.M. & Gould, R.O. *Acta Crystallogr. B* **51**, 423–431. (1995).
- Collaborative Computational Project, Number 4. *Acta Crystallogr. D* **50**, 760–763 (1994).
- Kleywegt, G.J. & Jones, T.A. SERC Daresbury Laboratory Study Weekend Proceedings, 59–66 (1994).
- Jones, T.A., Zou, J.Y., Cowan, S.W. & Kjeldgaard, M. *Acta Crystallogr. A* **47**, 110–119 (1991).
- Navaza, J. *Acta Crystallogr. A* **50**, 157–163 (1994).
- Brunger, A.T. *et al. Acta Crystallogr. D* **54**, 905–921 (1998).
- Esnouf, R.M. *J. Mol. Graph. Model* **15**, 132–143 (1997).
- Carson, M. *J. Appl. Crystallogr.* **24**, 958–961 (1991).
- Nicholls, A. *GRASP: graphical representation and analysis of surface properties.* (Columbia University, New York: 1993)